Research Article | Vol. 28, No. 22 / 26 October 2020 / Optics Express 33564
Optics EXPRESS

Mitigation of photon background in nanoplasmonic all-on-chip Raman sensors

KRISTOF REYNKENS,[1,2,*] STÉPHANE CLEMMEN,[1,2,3,4] ALI RAZA,[1,2] HAOLAN ZHAO,[1,2] JUAN SANTO-DOMINGO PEÑARANDA,[5] CHRISTOPHE DETAVERNIER,[5] AND ROEL BAETS[1,2]

[1]*Photonics Research Group, Department of Information Technology, Ghent University-IMEC, Technologiepark 126, 9052 Ghent, Belgium*
[2]*Center for Nano- and Biophotonics, Ghent University, 9052 Ghent, Belgium*
[3]*Laboratoire d'Information Quantique, Université Libre de Bruxelles, 1050 Brussels, Belgium*
[4]*OPERA-Photonique CP 194/5, Université Libre de Bruxelles (ULB), 1050 Brussels, Belgium*
[5]*Department of Solid State Sciences, CoCooN Research Group, Krijgslaan 281/51, Ghent 9000, Belgium*
[*]*kristof.reynkens@ugent.be*

Abstract: In the quest for a more compact and cheaper Raman sensor, photonic integration and plasmonic enhancement are central. Nanoplasmonic slot waveguides exhibit the benefits of SERS substrates while being compatible with photonic integration and mass-scale (CMOS) fabrication. A difficulty in pursuing further integration of the Raman sensor with lasers, spectral filters, spectrometers and interconnecting waveguides lies in the presence of a photon background generated by the excitation laser field in any dielectric waveguide constituting those elements. Here, we show this problem can be mitigated by using a multi-mode interferometer and a nanoplasmonic slot waveguide operated in back-reflection to greatly suppress the excitation field behind the sensor while inducing very little photon background.

1. Introduction

Raman spectroscopy has found an increasing number of applications during the last decades. To further extend its use, reducing the cost and size of Raman spectroscopy systems is essential. A typical Raman spectroscopic system consists of a spectrometer with cooled camera, a confocal microscope, a high power laser and spectral filters to remove that laser beam. The obvious answer to the demand for cheap and compact Raman systems lies in the nanophotonic integration of those elements on a single photonic chip. All the elements have indeed been demonstrated individually: spectrometers [1–3], lasers [4,5], spectral filters necessary to remove the strong excitation radiation [6] and also Raman sensors that boost the Raman response [7–9]. Recent progress [10–14] has been made regarding the Raman sensor itself by taking advantage of the evanescent field around a dielectric waveguide that allows an analyte to be probed over long optical path lengths. While this approach is effective in boosting the Raman signal, it also introduces an undesired photon background that ultimately reduces the signal-to-background ratio of any acquired Raman spectrum [15]. This photon background scales linearly with the intensity of the excitation beam and with the propagation length. The Raman-like background is generated both forward and backward and there is evidence that it is due to localized thermal fluctuations [16].

Plasmonic field enhancement is another notorious way to increase the Raman scattering and this effect also has been exploited for on-chip Raman spectroscopy, with antennas first [17] and plasmonic waveguides [18] soon later. Those plasmonic waveguides showed a level of Raman enhancement similar to the nanophotonic waveguides and share the same non-resonant (broadband) enhancement but without suffering from a significant photon background from a

#408638 https://doi.org/10.1364/OE.408638
Journal © 2020 Received 28 Aug 2020; revised 9 Oct 2020; accepted 13 Oct 2020; published 22 Oct 2020

Optics EXPRESS

waveguide dielectric. They therefore appear as the ideal option for a full Raman integrated system [19].

Proceeding to integrate this sensor with a circuit capable of analyzing the Raman scattered light demands that no further inelastic scattering or photoluminescence occurs in the circuit surrounding the sensor. Unfortunately, the Raman-like background from the dielectric waveguide (in our case a silicon nitride waveguide [16]) becomes significant over propagation distances that can easily exceed millimeters for spectral filters [6] or AWG. The resulting background ultimately limits the concentration of analytes that can be probed because of the shot noise associated to it. That is the reason why previous characterisation [18] used a minimalistic input waveguide as the only interface between the facet of the chip (where an external excitation beam is focused) and the Raman plasmonic sensor itself. The study clearly showed that the signal-to-noise ratio was critically dependant on the length of that access waveguide so that it could not be combined with a "conventional" spectral notch filter such as Bragg gratings [6] placed after the sensor.

In order to separate the Raman scattered light from the excitation beam without inducing a spurious photon background, we propose to use a multi-mode interferometer (MMI) [20] and backward Raman collection. In Fig. 1, we see that the MMI lets the excitation beam propagate from the input facet to the sensor and then lets the Raman back-scattered light propagate from the sensor to an output waveguide, while the excitation beam and associated background from the entrance waveguide keep on forward propagating in the plasmonic sensor and are finally absorbed. Of course, this approach induces an intrinsic 3dB loss for the Raman scattered light from the sensor. Despite this, the architecture is beneficial because the MMI is short (112 μm) (therefore inducing little Raman-like background) and it is also highly multimode so that most of that spurious radiation actually does not couple to the output port. In theory, using a circulator over an MMI would be even better since it would collect 100% of the backscattered Raman light. However in practice, integrated circulators are difficult to implement and they typically have a power penalty of > 3dB associated with them [21].

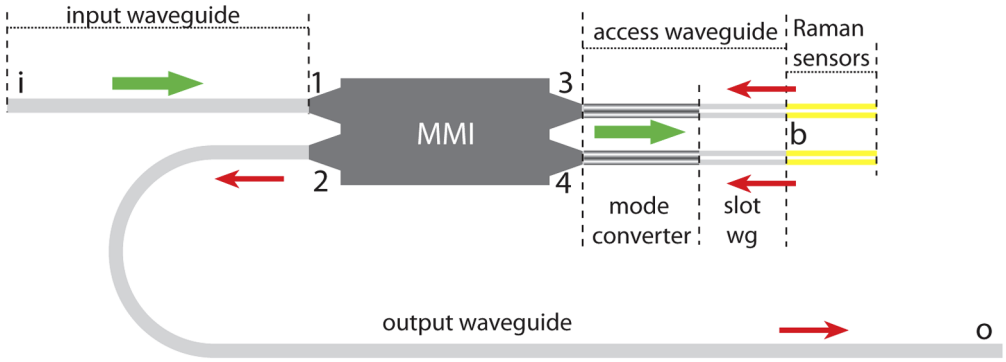

Fig. 1. Schematic of the configuration relying on two nanoplasmonic Raman sensors and a MMI separating the forward-propagating excitation beam (green arrow) from the backward-propagating Raman scattered light (red arrows). Grey elements are made of Si_3N_4 while yellow elements are primarily made of gold. The MMI and the Raman sensing plasmonic slot waveguides are linked by an access waveguide made of a mode converter (grey gradient section), and a dielectric slot waveguide (grey and white).

In this paper, we first describe our design and its fabrication. Then we discuss our measurement setup and procedure. Afterwards we present the results obtained after which we give some outlooks and concluding remarks.

Optics EXPRESS

2. Methods

2.1. Design

Our architecture relies on a 2×2 multimode interferometer (MMI) [22]. The two left ports (labeled 1 and 2 in Fig. 1) are the input and output of our system. As an MMI is a linear and reciprocal element, having a single output port (labeled 3) necessarily translates into extra loss either from port 1 to 3 or from port 3 to 2 (at a given wavelength). However two output ports (labeled 3 and 4), having a splitting ratio of 50 : 50 maximizes the overall transmission from port 1 to ports 3 and 4, and then from those two ports to port 2. In that case, the input excitation power is optimally used if we place a Raman sensor at each of the two output ports of the MMI. Our MMI is designed via eigenmode expansion using Lumerical 's commercial solver and by taking the thickness (300 nm) and the refractive index of the Si_3N_4 layer ($n = 1.89$ at a wavelength of 830 nm) as fixed parameters. The designed in-plane dimensions of the balanced MMI are $w \times l = 8.9 \times 112.5\ \mu m^2$. This results in a balanced MMI designed at a central wavelength of 830 nm and a 3 dB bandwidth of 220 nm. The MMI is complemented at each port by a 16.5 μm long taper allowing a good mode matching between the mode of the waveguide and the mode of the MMI, thereby reducing spurious reflections. The MMI is preceded by a 300 μm-long strip waveguide (input waveguide) having a cross-section $w \times t = 550 \times 300\ nm^2$. The MMI and plasmonic Raman sensors are connected together via a mode converter matching the rib waveguide mode to the slot waveguide mode and a short section of dielectric slot waveguide. In an ideal situation, the mode converter and the dielectric slot waveguide are the only ones that contribute to the photon background as they are expected to scatter photons backward in the same way the nanoplasmonic sensors generates the Raman light. The mode converter is 20 μm long and the short section of dielectric slot waveguide varies from sample to sample from 23.5 to 116 μm. The width of the slot waveguide is 700 nm including a gap of 150 nm. In the rest of this work the mode converter and dielectric slot waveguide will be taken together and described as one single waveguide: the access waveguide. While the entire circuit (input/output waveguide, MMI and access waveguide) is cladded with 2 μm of silica on the top, the Raman sensor and a fraction of the dielectric slot waveguide are open to the air. To avoid a poor mode matching at the silica-air interface, the air is replaced by water during our measurements.

As our configuration collects backward-scattered Raman light, there is no optimal length for the plasmonic waveguides and the Raman signal simply saturates as the excitation beam decays due to propagation loss. Therefore, we choose to have a plasmonic slot waveguide length of 55 μm-long which far exceeds the decay length of the pump field (1.8 μm). The nanoplasmonic slot has a nominal gap width of 15 nm as reported previously [18]. The output waveguide has the same cross section as the input waveguide. This waveguide is taken purposely long (11 mm) to demonstrate the possibility offered by our architecture. In the future, that waveguide can include spectral functionalities e.g. a pump rejection filter [6].

2.2. Fabrication

The photonic circuits used for experiments are fabricated on 200 mm silicon wafers [23]. 300 nm SiN is deposited through a low temperature plasma enhanced chemical vapor deposition process [24] on a 3.3 μm silica layer. Patterning is performed by deep UV-lithography and reactive ion etching. The nanoplasmonic slots are fabricated by conformally covering the SiN slot waveguides with 60 nm Al_2O_3 using ALD (in order to reduce the width of the slot gap) followed by the sputtering of a 2 nm Ti adhesion layer and a 5.5 nm gold layer along the side walls of the slot. A more detailed description of the fabrication can be found in [18].

Samples have been prepared that differ in the length of the dielectric slot waveguide between the MMI and the Raman sensor. This results in access waveguide lengths of 43.5 and 136 μm. Two structures having the same length are fabricated on the same die for a total of four samples.

Optics EXPRESS

The samples are functionalized with an analyte of 4-Nitrothiophenol (NTP) that binds selectively to the gold sensor. Further details about it can be found in [19].

2.3. Setup and measurements

SERS spectra of the samples are acquired on the measurement setup depicted in Fig. 2. The excitation CW laser light (785 nm) is provided by an XTRA II laser. A spectral filter is used in order to clean its spectrum. A polarizing beamsplitter ensures that only the TE-polarized light is transmitted towards the chip while the half-wave plate provides control over the amount of pump power. The light is coupled into and out of the chip by two identical Mitutoyo Plan Apo objectives (50×, NA=0.65). A dichroic mirror suppresses the residual excitation beam while transmitting the Raman scattered light. Finally, the light is captured in a collimator and guided in a multimode fiber towards the spectrometer (Shamrock 303i spectrometer with a Andor iDus 416 deep-cooled CCD camera).

Spectra are acquired for durations ranging from 60 to 180 seconds and excitation powers from 6 to 25 mW (measured before the objective). The excitation power is limited in order to prevent the photoreduction of NTP into a form of dimercaptoazobenzene (DMAB). A droplet of water is applied on top of the plasmonic slots when performing the acquisition. This allows a better mode matching at the interface of the cladded and uncladded parts of the circuit.

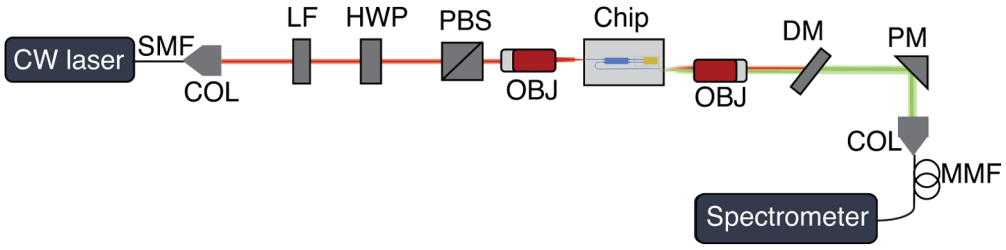

Fig. 2. Schematic of the setup used to measure the SERS spectra. SMF: single-mode fiber, COL: collimator, LF: line filter, HWP: half-wave plate, PBS: polarizing beamsplitter, OBJ: objective , DM: dichroic mirror, PM: parabolic mirror, MMF: multimode fiber.

A typical spectrum acquired with our plasmonic sensor is presented in Fig. 3(a). It displays the characteristic peaks associated to NTP. The spectrum is presented with the dark counts subtracted. As the noise associated to the dark counts cannot be subtracted, we choose the acquisition parameters so that this noise is far lesser than other sources of noise. The spectrum displays the noticeable photon background we referred to in the introduction. To compare various results, we define the signal-to-background ratio (SBR) as the integrated number of counts (S) in the main peak (corresponding to 1341 cm^{-1} NTP-mode, shaded in green) by the integrated number of counts due to the photon background (BG) integrated over the same spectral span (shaded in red).

Defining a SBR rather than the signal-to-noise ratio is more relevant when parameters such as excitation power, incoupling loss, or acquisition time are varied. The SBR is independent of those factors. The SBR depends however on how well the signal and the background spectrum can be separated. That separation is perfect if the spectrum of the spurious photon background is completely known and if there would be no shot noise associated to both the background and the Raman scattered light. In the present case, we assume the background follows a purely linear trend over the integration span corresponding to the NTP peak at 1341 cm^{-1}. That approximation and the presence of the shot noise induces an uncertainty (relative standard deviation) of 12% on the SBR values we provide.

Optics EXPRESS

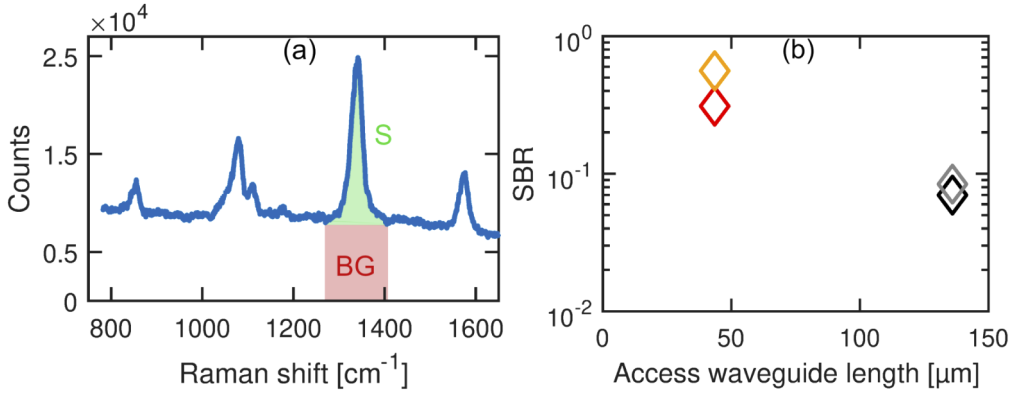

Fig. 3. (a) Measured Raman spectrum of NTP using our photonic-plasmonic sensor (Fig. 1) with the instrumentation noise subtracted. The spectrum shows the characteristic NTP features (855 cm^{-1}, 1111 cm^{-1}, 1341 cm^{-1}, 1575 cm^{-1}) [25]. The green and red regions indicate the integration range used in the SBR calculation. (b) The signal-to-background ratio for our four photonic-plasmonic sensors.

3. Results and discussion

Figure 3(a) clearly shows the presence of a remaining photon background. We expect this background to be due to the access waveguide between the MMI and the plasmonic waveguide. We therefore measure the effects of its length on the SBR. The results presented in Fig. 3(b) show that indeed the longest access (136 μm) waveguide is associated to a reduced SBR because the background increases. In an ideal MMI-plasmonic slot hybrid this contribution due to the access waveguide would be the only major background source. However unwanted back-reflections at the interface between the dielectric and plasmonic slot, the interface between the MMI-taper and the mode converter, the interface between the mode converter and the slot waveguide or the interface between the silica cladded part of the dielectric slot waveguide and the water cladded part of that same waveguide can reflect a small portion of the excitation beam into the output waveguide. Through numerical simulation, the reflection at the plasmonic sensor interface is expected to be at least 10 dB larger than the other reflections.

While the length of the access waveguide could be reduced further, it does not necessarily lead to a reduced background if the reflectivity of the nanoplasmonic sensor becomes significant. Indeed, the reflected excitation beam will eventually reach the long output waveguide where it will generate a photon background. To quantify the importance of that undesired reflection on the SBR, we measured it for two output waveguide lengths on the same chip: 11 mm and 5 mm. Figure 4 presents the result of that measurement. We display the ratio (R) of the SBR when the output waveguide is the longest (11 mm) to the SBR when the output waveguide is only 5 mm. This ratio is therefore immune to fabrication variations occurring for chips sputtered with different conditions. The fact that this ratio is smaller than unity indicates that some spurious photon generation occurs in the output waveguide. The fact that it goes asymptotically to 1 when increasing the access waveguide to 100's of micrometers indicates that the background contribution due to the access waveguide length is strongly dominant in that case. At the opposite side, if the background contribution due to the output waveguide was strongly dominant, this ratio would be 46% (5 mm/11 mm).

For the structures with the short access waveguide the ratio R is 0.83, showing that the background due to the access waveguide and the output waveguide are of the same order. Other background sources due to the MMI and the input waveguide don't seem to play a major role

Optics EXPRESS

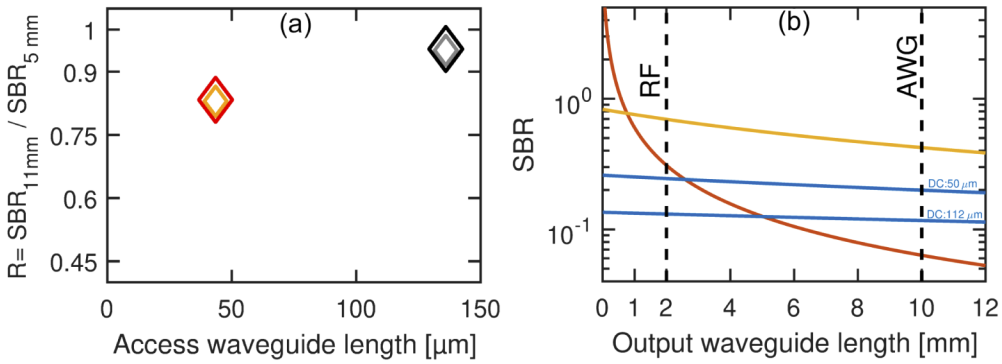

Fig. 4. (a) Decrease in SBR when increasing the output waveguide length from 5 mm to 11 mm for the four samples. (b) Evolution of the signal-to-background ratio with the length of the output waveguide for the case of the MMI-based configuration (yellow curve) compared to the simpler "transmission configuration" (red curve) and a directional coupler-based configuration (blue curves) with a DC length of 50 μm & 112 μm respectively. The dashed lines illustrate the typical length of elements that could be integrated to the plasmonic Raman sensor: rejection filter (RF) [6] and arrayed waveguide grating (AWG) [3].

under the device dimensions probed. If they did, R would be approaching unity for all the structures as changing the output waveguide length would not affect it.

The fact that the background contribution due to the 11 mm output waveguide is nearly equal to the 43.5μm access waveguide is already an encouraging results. It shows we can integrate elements such as a notch filter [6] to remove the excitation beam by paying a low price in term of the SBR: a reduction by a factor of 2 (hence a reduction of the SNR by $\sqrt{2}$). As the length of the access waveguide can easily be reduced to the length of the mode converter (20 μm), we can conclude that the actual limitation of our architecture lies in the reflections arising at the interface between the dielectric and plasmonic slot waveguides. Before discussing how to further improve this, we are comparing this architecture with the simplest architecture possible.

In order to integrate the Raman sensor with other elements, the alternative to our architecture consists of placing the elements behind the sensor and collecting the forward-scattered Raman light. We refer to that configuration as the "transmission configuration". To make a comparison, we assume a circuit for the transmission configuration with a plasmonic slot waveguide of optimal length (1.8 μm [15]). The amount of Raman scattered power can then be taken equal in both configurations. In the case of the MMI-based circuit, we consider the photon-background contribution due to the access waveguide with a length of 43.5 μm (our best demonstrated sample) and the contribution due the output waveguide. As we know the amount of photon background generated per unit of length and per unit of optical power of the excitation beam, we can predict the amount of this photon background as a function of the output waveguide length. This requires knowledge of the fraction of the excitation laser beam power reflected to the output port. We estimated experimentally this reflection to be between -26.9 dB and -32 dB for our various samples. From simulation, those numbers are between - 25 dB and - 30 dB where the uncertainty reflects the imprecise knowledge of the gold thickness. Because the excitation power is reduced, the photon background contribution of the output waveguide is 173 times weaker per unit of length than the contribution due to the access waveguide. For simplicity, we assumed the MMI to be perfectly balanced both at the excitation and Raman scattered wavelengths.

In the case of the transmission configuration, we can proceed to the same reasoning but we have to make an assumption on the transmission of the pump and of the Raman scattered light through the plasmonic slot waveguide. We take this transmission to be -12.22 dB (coupling

Optics EXPRESS

loss of -3.95 dB/facet and absorption loss of -2.4 $dB/\mu m$ [18]). The result of the comparison is plotted in Fig. 4(b) via the expected SBR corresponding to both configurations. It can be seen that the SBR of the MMI-based configurations outperforms the transmission configuration for an output waveguide length as short as 765 μm despite the current (not optimized) geometry of the access waveguide length. This MMI configuration thus proves to be a good option for further integration with spectral functionalities. It also eases the fabrication because collecting the back-scattered Raman light implies that the length of the nanoplasmonic waveguide does not need to be optimized while it requires to be precisely controlled for the forward-scattering case [15].

We can conclude that our MMI provides a significant advantage over the before mentioned transmission measurement and comes at nearly no cost. One could however argue that the same would apply to a balanced directional coupler (DC) with a 50/50 splitting ratio. This is not the case because a directional coupler comes with a significant photon background noise penalty. As a DC is simply made of two single-mode waveguides and as we know the quantity of background photons generated in such a waveguide per unit of length [15,16], the effect on the SBR can be deduced for a DC with the same length as the MMI (112 μm) and a more compact DC with a length in the order of 50 μm [26]. The result of that calculation can be seen in Fig. 4(b). It shows indeed that the SBR is between 2 and 6 times better for the MMI-case as compared to the DC-case, depending on output waveguide length and DC-length.

The fact that our MMI provides a better SBR is because the photon background originating from it is small enough to be negligible compared to background generated in the access and output waveguide. This can be understood when considering the multimode behaviour of the MMI. If only the modes with TE polarization are considered then the MMI supports 24 different guided modes. As a result the generated background photons, which are incoherent relative to each other, couple to all those modes and will upon propagation to the output of the MMI not be confined to the output waveguides. This is further confirmed by the fact that only 5 out of those 24 modes are responsible for supporting 90% of the transmission of in-coupled to out-coupled signal. Therefore most of the background generated in the MMI will be radiated out rather than being collected at the output waveguide. The effect will be similar for the TM modes. This clearly demonstrates the benefit of using an MMI rather than a directional coupler.

4. Outlook and conclusion

The architecture presented here can be improved in several way. One route for improvement consists in further reducing the length of the access waveguide. It is nearly trivial to reduce its length to the length of the mode converter (20 μm). Reducing the length of the mode converter is not as trivial because there is a trade-off between a shorter length and proper mode matching. Moreover, we know that for access waveguides shorter than 43.5 μm, the reflection of the excitation beam is the actual limitation. In the current study, we have no possibility to experimentally distinguish (1) the reflection due to the interface between the dielectric and plasmonic slot waveguides from (2) the reflection due to the mode converter itself or even (3) the reflections occurring at the interface between the silica cladded and water cladded slot waveguide. From numerical simulation, it is expected that the reflection due to the plasmonic waveguide (1) is at least 10 dB larger than the other two sources. More advanced mode matching at those three critical points will ultimately reduce the reflection and therefore improve the performance of our MMI-based circuit. For instance, the reflection due to the plasmonic waveguide could be better controlled by a more precise deposition technique such as the atomic layer deposition of gold that furthermore results in an increased Raman response [27]. Another way to improve the architecture is to engineer the MMI so that it acts as a wavelength division multiplexer [28,29] transmitting the excitation beam from a port 1 to 3 with a high transmission and transmitting it inefficiently from port 3 to port 2 while the scattered Raman light is collected in port 3. This

Optics EXPRESS

would lead to a reduction of the reflected pump light in the output waveguide therefore improving the SBR for even longer/more complex analyzing circuits.

In conclusion, our novel configuration based on a 2×2 MMI works effectively. It allows to extract the Raman scattered light out of a Raman sensor while enabling further integration with an analysing photonic circuit i.e. lasers, filters and spectrometers which are required for a complete Raman-on chip spectrometer. The penalty in terms of extra photon background generated is minimal. The background was shown to originate from back-scattered Raman background in the short access waveguide linking the MMI to the Raman sensor and from the output waveguide. The photon flux generated in that output waveguide is due to the same process occurring in the forward direction as the result of the presence of a remaining excitation beam. We found no contribution of the MMI on the photon background. This is an advantage of the MMI over a directional coupler that is able to perform the same functionality. We discussed the possible improvement to our work and showed that the focus should be put on reducing spurious reflections of the excitation beam on its path to the Raman sensor. In the future, an MMI having a spectral functionality may help to improve the capability of our architecture further.

Funding

Vlaamse regering (Methusalem grant (R. Baets) "Smart Photonic Chips); Fonds De La Recherche Scientifique - FNRS.

Disclosures

The authors declare no conflicts of interest.

References

1. X. Nie, E. Ryckeboer, G. Roelkens, and R. Baets, "Cmos-compatible broadband co-propagative stationary fourier transform spectrometer integrated on a silicon nitride photonics platform," Opt. Express **25**(8), A409–A418 (2017).
2. E. Ryckeboer, X. Nie, A. Z. Subramanian, D. Martens, P. Bienstman, S. Clemmen, S. Severi, R. Jansen, G. Roelkens, and R. Baets, "Cmos-compatible silicon nitride spectrometers for lab-on-a-chip spectral sensing," Proc. SPIE **9891**, 98911K (2016).
3. D. Martens, A. Z. Subramanian, S. Pathak, M. Vanslembrouck, P. Bienstman, W. Bogaerts, and R. G. Baets, "Compact silicon nitride arrayed waveguide gratings for very near-infrared wavelengths," IEEE Photonics Technol. Lett. **27**(2), 137–140 (2015).
4. S. Kumari, E. P. Haglund, J. S. Gustavsson, A. Larsson, G. Roelkens, and R. G. Baets, "Vertical-cavity silicon-integrated laser with in-plane waveguide emission at 850 nm," Laser Photonics Rev. **12**(2), 1700206 (2018).
5. E. Haglund, M. Jahed, J. S. Gustavsson, A. Larsson, J. Goyvaerts, R. Baets, G. Roelkens, M. Rensing, and P. O'Brien, "High-power single transverse and polarization mode vcsel for silicon photonics integration," Opt. Express **27**(13), 18892–18899 (2019).
6. X. Nie, N. Turk, Y. Li, Z. Liu, and R. Baets, "High extinction ratio on-chip pump-rejection filter based on cascaded grating-assisted contra-directional couplers in silicon nitride rib waveguides," Opt. Lett. **44**(9), 2310–2313 (2019).
7. A. Dhakal, A. Z. Subramanian, P. Wuytens, F. Peyskens, N. Le Thomas, and R. Baets, "Evanescent excitation and collection of spontaneous raman spectra using silicon nitride nanophotonic waveguides," Opt. Lett. **39**(13), 4025–4028 (2014).
8. A. Dhakal, P. C. Wuytens, F. Peyskens, K. Jans, N. L. Thomas, and R. Baets, "Nanophotonic waveguide enhanced raman spectroscopy of biological submonolayers," ACS Photonics **3**(11), 2141–2149 (2016).
9. S. A. Holmstrom, T. H. Stievater, D. A. Kozak, M. W. Pruessner, N. Tyndall, W. S. Rabinovich, R. A. McGill, and J. B. Khurgin, "Trace gas raman spectroscopy using functionalized waveguides," Optica **3**(8), 891–896 (2016).
10. H. Zhao, S. Clemmen, A. Raza, and R. Baets, "Stimulated raman spectroscopy of analytes evanescently probed by a silicon nitride photonic integrated waveguide," Opt. Lett. **43**(6), 1403–1406 (2018).
11. N. F. Tyndall, T. H. Stievater, D. A. Kozak, K. Koo, R. A. McGill, M. W. Pruessner, W. S. Rabinovich, and S. A. Holmstrom, "Waveguide-enhanced raman spectroscopy of trace chemical warfare agent simulants," Opt. Lett. **43**(19), 4803–4806 (2018).
12. D. A. Coucheron, D. N. Wadduwage, G. S. Murugan, P. T. So, and B. S. Ahluwalia, "Chip-based resonance raman spectroscopy using tantalum pentoxide waveguides," IEEE Photonics Technol. Lett. **31**(14), 1127–1130 (2019).
13. F. Peyskens, A. Z. Subramanian, P. Neutens, A. Dhakal, P. Van Dorpe, N. Le Thomas, and R. Baets, "Bright and dark plasmon resonances of nanoplasmonic antennas evanescently coupled with a silicon nitride waveguide," Opt. Express **23**(3), 3088–3101 (2015).

Optics EXPRESS

14. H. Zhao, B. Baumgartner, A. Raza, A. Skirtach, B. Lendl, and R. Baets, "Multiplex volatile organic compound raman sensing with nanophotonic slot waveguides functionalized with a mesoporous enrichment layer," Opt. Lett. **45**(2), 447–450 (2020).
15. A. Raza, S. Clemmen, P. Wuytens, M. de Goede, A. S. K. Tong, N. L. Thomas, C. Liu, J. Suntivich, A. G. Skirtach, S. M. Garcia-Blanco, D. J. Blumenthal, J. S. Wilkinson, and R. Baets, "High index contrast photonic platforms for on-chip raman spectroscopy," Opt. Express **27**(16), 23067–23079 (2019).
16. N. Le Thomas, A. Dhakal, A. Raza, F. Peyskens, and R. Baets, "Impact of fundamental thermodynamic fluctuations on light propagating in photonic waveguides made of amorphous materials," Optica **5**(4), 328–336 (2018).
17. F. Peyskens, A. Dhakal, P. Van Dorpe, N. Le Thomas, and R. Baets, "Surface enhanced raman spectroscopy using a single mode nanophotonic-plasmonic platform," ACS Photonics **3**(1), 102–108 (2016).
18. A. Raza, S. Clemmen, P. Wuytens, M. Muneeb, M. Van Daele, J. Dendooven, C. Detavernier, A. Skirtach, and R. Baets, "Ald assisted nanoplasmonic slot waveguide for on-chip enhanced raman spectroscopy," APL Photonics **3**(11), 116105 (2018).
19. N. Turk, A. Raza, P. Wuytens, H. Demol, M. Van Daele, C. Detavernier, A. Skirtach, K. Gevaert, and R. Baets, "Comparison of free-space and waveguide-based sers platforms," Nanomaterials **9**(10), 1401 (2019).
20. D. M. Kita, J. Michon, and J. Hu, "A packaged, fiber-coupled waveguide-enhanced raman spectroscopic sensor," Opt. Express **28**(10), 14963–14972 (2020).
21. Y. Zhang, Q. Du, C. Wang, T. Fakhrul, S. Liu, L. Deng, D. Huang, P. Pintus, J. Bowers, C. A. Ross, J. Hu, and L. Bi, "Monolithic integration of broadband optical isolators for polarization-diverse silicon photonics," Optica **6**(4), 473–478 (2019).
22. L. B. Soldano and E. C. Pennings, "Optical multi-mode interference devices based on self-imaging: principles and applications," J. Lightwave Technol. **13**(4), 615–627 (1995).
23. A. Rahim, J. Goyvaerts, B. Szelag, J. Fedeli, P. Absil, T. Aalto, M. Harjanne, C. Littlejohns, G. Reed, G. Winzer, S. Lischke, L. Zimmermann, D. Knoll, D. Geuzebroek, A. Leinse, M. Geiselmann, M. Zervas, H. Jans, A. Stassen, C. Domanguez, P. Munoz, D. Domenech, A. L. Giesecke, M. C. Lemme, and R. Baets, "Open-access silicon photonics platforms in europe," IEEE J. Sel. Top. Quantum Electron. **25**(5), 1–18 (2019).
24. A. Z. Subramanian, P. Neutens, A. Dhakal, R. Jansen, T. Claes, X. Rottenberg, F. Peyskens, S. Selvaraja, P. Helin, B. Du Bois, K. Leyssens, S. Severi, P. Deshpande, R. Baets, and P. Van Dorpe, "Low-loss singlemode pecvd silicon nitride photonic wire waveguides for 532–900 nm wavelength window fabricated within a cmos pilot line," IEEE Photonics J. **5**(6), 2202809 (2013).
25. P. Du, X. Zhang, H. Yin, Y. Zhao, L. Liu, Z. Wu, and H. Xu, "In situ surface-enhanced raman scattering monitoring of reduction of 4-nitrothiophenol on bifunctional metallic nanostructure," Jpn. J. Appl. Phys. **57**(3), 030308 (2018).
26. S. Nevlacsil, M. Eggeling, P. Muellner, G. Koppitsch, M. Sagmeister, J. Kraft, and R. Hainberger, "Broadband sin asymmetric directional coupler for 840 nm operation," OSA Continuum **1**(4), 1324–1331 (2018).
27. M. Van Daele, M. B. E. Griffiths, A. Raza, M. M. Minjauw, E. Solano, J.-Y. Feng, R. K. Ramachandran, S. Clemmen, R. Baets, S. T. Barry, C. Detavernier, and J. Dendooven, "Plasma-enhanced atomic layer deposition of nanostructured gold near room temperature," ACS Appl. Mater. Interfaces **11**(40), 37229–37238 (2019).
28. S. Triki, M. Najjar, and H. Rezig, "Optimization of mmi-wdm demultiplexer by using bpm method," in *ICTON Mediterranean Winter Conference*, (IEEE, 2007), pp. 1–6.
29. T. D. Bucio, A. Z. Khokhar, G. Z. Mashanovich, and F. Y. Gardes, "N-rich silicon nitride angled mmi for coarse wavelength division (de) multiplexing in the o-band," Opt. Lett. **43**(6), 1251–1254 (2018).